Supplementary Information

MoP@NiCo-LDH on nickel foam as bifunctional electrocatalyst for high efficiency water and urea-water electrolysis

Tuo Wang [a], Huimin Wu [a, *], Chuanqi Feng [a], Lei Zhang [b, *], Jiujun Zhang [c]

[a.] *Ministry-of-Education Key Laboratory for the Synthesis and Application of Organic Functional Molecules, Hubei Key Laboratory of Polymer Materials, National & Local Joint Engineering Research Center of High-throughput Drug Screening Technology, Key Laboratory of regional development and environmental response in Hubei Province, Faculty of Resources and Environmental Science, College of Chemistry & Chemical Engineering, Hubei University, Wuhan 430062, PR China*

[b.] *Energy, Mining and Environment, National Research Council of Canada, Vancouver, Canada V6T 1W5*

[c.] *Institute for Sustainable Energy / College of Sciences, Shanghai University, Shanghai, China 200444*

*Corresponding author.

Email address: whm267@hubu.edu.cn; Lei.Zhang@nrc-cnrc.gc.ca

Table of contents

Ⅰ XRD patterns of MoP@NiCo-LDH/NF-x

Figure S1 shows the XRD patterns of MoP@NiCo-LDH/NF-x (x=10, 20, 30 minutes). The diffraction peaks at 27.9°, 32.2°, 41.2°, 57.5°, and 74.3° correspond to the (001), (100), (101), (110) and (201) planes of MoP (JCPDS No.24-0771). The peaks at 11.5°, 23.0°, 35.0°, 39.2°, 39.5°, 60.8°, and 62.5° adopt to the crystal planes (003), (006), (012), (015), (110) and (113) of NiCo-LDH (JCPDS No.40-0216) respectively. The peaks at 44.5°, 51.8°, and 76.6° are indexed to nickel foam (NF) (JCPDS No.40-0850). It can be seen that the diffraction peaks in MoP@NiCo-LDH/NF formed under different electrodeposition times are corresponded to standard cards.

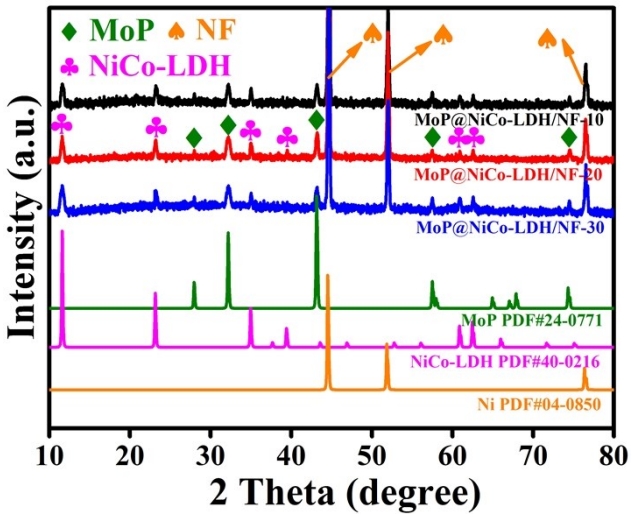

Figure S1. XRD patterns of MoP@NiCo-LDH/NF-x.

Ⅱ SEM images of NF, MoP/NF, and NiCo-LDH/NF

Figure S2 shows the SEM images of NF (a), MoP/NF (b), and NiCo-LDH/NF (c). The inset is to show the higher magnification. It can be seen that the NF is a skeleton with smooth surface (a, b). After MoP is grown on it, the surface is no longer smooth, forming a structure of homogeneous block layer partition (c, d). When NiCo-LDH/NF is formed by direct electrodeposition on base NF, the pleated and lamellar tremella cluster structure (e, f) characteristic of LDH could be clearly seen.

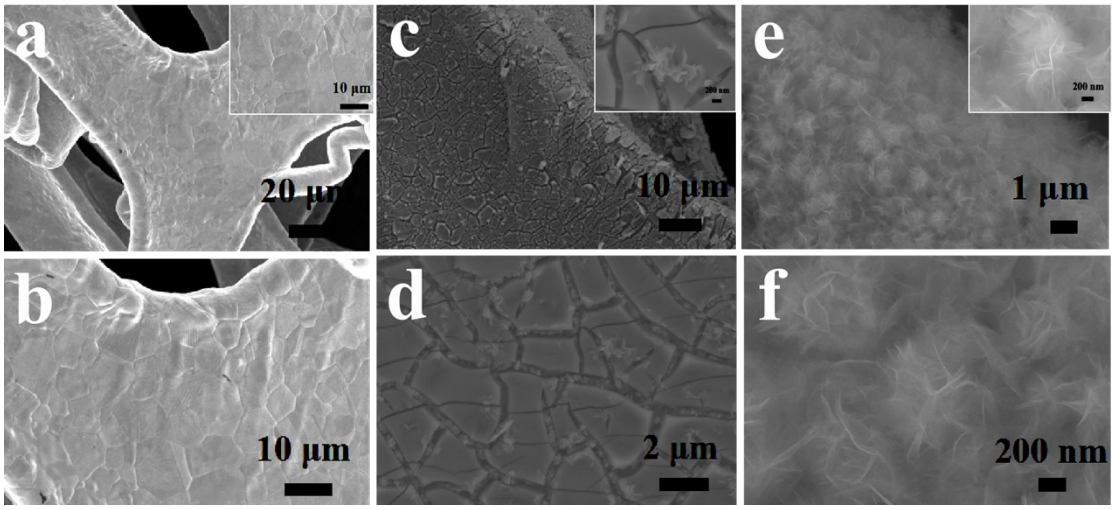

Figure S2. SEM images of NF (a and b), MoP/NF (c and d), and NiCo-LDH/NF (e and f). Inset is to show the higher magnification.

Ⅲ SEM images of MoP@NiCo-LDH/NF-x

Figure S3 (a-c) shows the SEM images of MoP@NiCo-LDH/NF-x. Obviously, all the samples show the folded and flaky structure, but the morphology is slightly different at different deposition times, indicating that the electrodeposition time has a certain influence on the morphology of the catalyst. Proper deposition time can increase the specific surface area of catalyst to a certain extent, but when the deposition time exceeds a certain value, it has a negative effect. It can be seen from MoP@NiCo-LDH/NF-10, the formation of uniform distribution on the base of fold layer, as the electrodeposition time increases to 20 minutes, fold lamellas gather themselves together, and gradually form fold tremella clusters, which can increase the specific surface area. But when time increases to 30 minutes, this kind of tremella clusters gradually gather together, form a dense compact clusters of tremella shape, which reduces the specific surface area. MoP@NiCo-LDH/NF-20 has the larger specific surface area, which has the relatively more active sites on the surface.

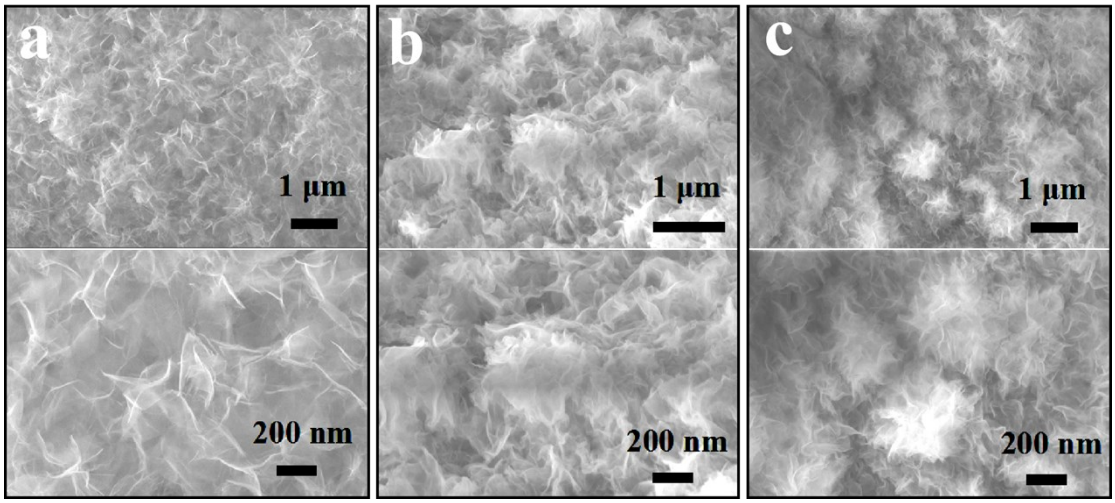

Figure S3. SEM images of MoP@NiCo-LDH/NF-x.

Ⅳ EDX spectrum of MoP@NiCo-LDH/NF-20

Figure S4 shows EDX spectrum of MoP@NiCo-LDH/NF-20. It can be seen from the figure that MoP@NiCo-LDH/NF-20 is composed of four elements (except the C and O elements in the air), including Mo, P, Ni, and Co. The interpolated table shows the elements atom ratio from EDX investigation. And the proportion content of each element in the material is different from that of the initial quantity (because of the existence of the substrate, all the inputs in the solution cannot completely grow on the substrate). Among them, the molar ratio of Mo and P is not 1:1, because Mo/NF is first generated in NF, and then after phosphating to produce MoP/NF, only the surface of Mo precursor/NF can be phosphated.

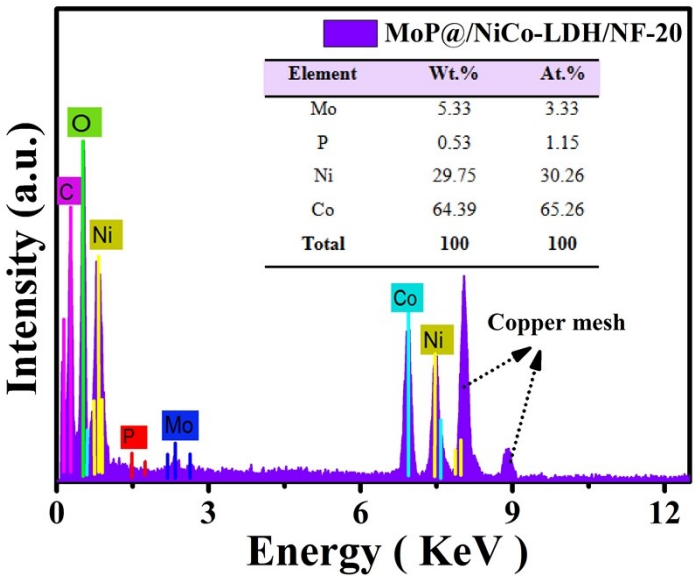

Figure S4. EDX spectrum of MoP@NiCo-LDH/NF-20.

Ⅴ LSV curves and Nyquist plots of MoP@NiCo-LDH/NF-x

Figure S5 (a-b) shows LSV curves for the UOR (a) and HER (b) of MoP@NiCo-LDH/NF-x. It can be seen from the figure that as the potential increases, the current density also increases gradually. At any of the same potentials in the interval, the MoP@NiCo-LDH/NF-20 has a higher current density, indicating that the MoP@NiCo-LDH/NF-20 has the better catalytic performance. **Figure S5(c)** shows Nyquist plots of MoP@NiCo-LDH/NF-x in the frequency range of 1-10^5 Hz. It is clear that MoP@NiCo-LDH/NF-20 has a minimum R_{ct}, indicating a faster charge transfer rate, which may also be the reason why MoP@NiCo-LDH/NF-20 has better UOR and HER catalytic performance.

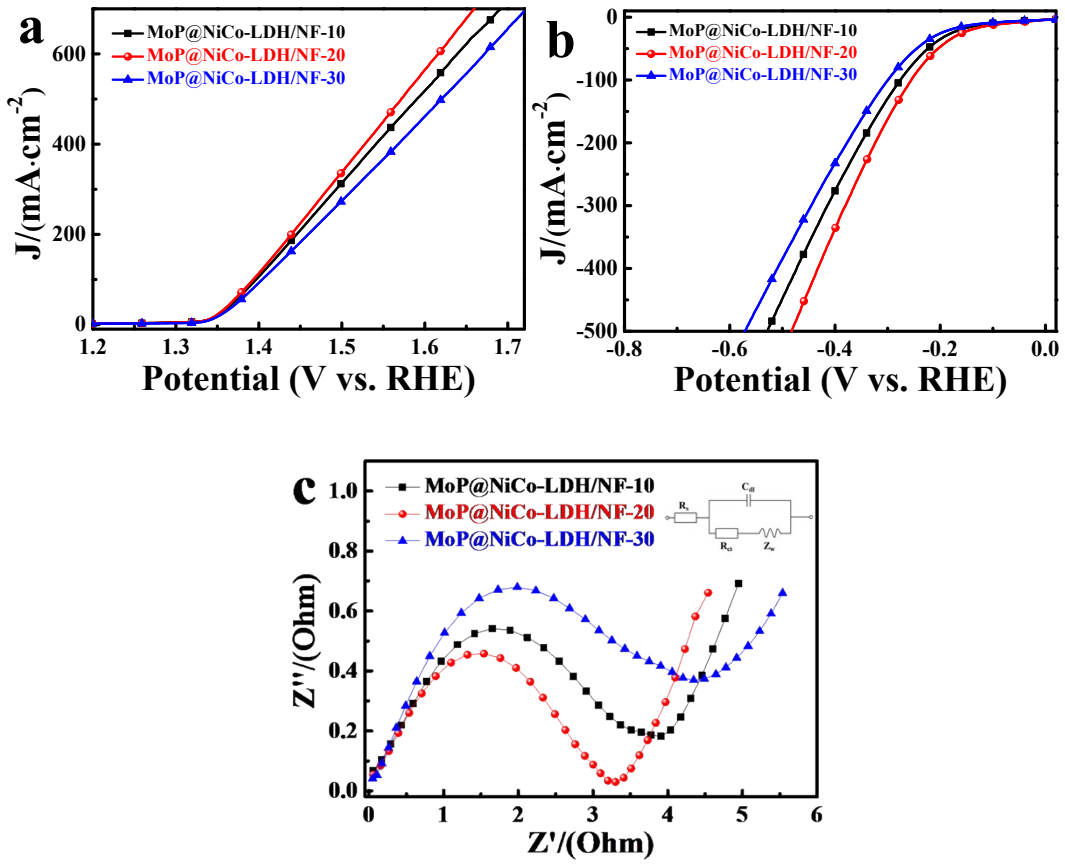

Figure S5. LSV curves for the UOR (a) and HER (b) of MoP@NiCo-LDH/NF-x. (c)Nyquist plots of MoP@NiCo-LDH/NF-x in the frequency range of 1-10^5 Hz. Inset is an equivalent circuit.

Ⅵ UOR and HER performance data at 100 mA cm^{-2}

Table S1. UOR and HER performance data at 100 mA cm^{-2}

Materials	UOR		HER		Cell Voltage (V)	C_{dl} (mF cm^{-2})	R_{ct} (Ω)
	Potential (V)	Tafel slope (mV dec^{-1})	Potential (mV)	Tafel slope (mV dec^{-1})			
NF	>1.56	50	495	189	-	-	10.3
MoP/NF	1.404	44	326	152	1.494	35.3	5.1
NiCo-LDH/NF	1.429	47	373	165	1.579	10.1	7.3
MoP@NiCo-LDH/NF-20	1.392	40	255	145	1.405	70.1	3.2
IrO_2/NF	1.625	82	-	-	1.708*	-	-
Pt/C/NF	-	-	170	49		-	-

*1.708 V is the cell voltage of Pt/C/NF||IrO_2/NF.

Table S1 shows the UOR and HER performance data of NF, MoP/NF, NiCo-LDH/NF, MoP@NiCo-LDH/NF-20, IrO_2/NF, and Pt/C/NF at 100 mA cm^{-2}. The electrode potentials of NF, MoP/NF, NiCo-LDH/NF, MoP@NiCo-LDH/NF-20, and IrO_2/NF towards UOR are >1.56, 1.473, 1.404, 1.429, 1.932, and 1.625 V. The Tafel slopes of NF, MoP/NF, NiCo-LDH/NF, MoP@NiCo-LDH/NF-20, and IrO_2/NF towards UOR are 50, 48, 44, 47, 40, and 82 mV dec^{-1}. The electrode potentials of NF, MoP/NF, NiCo-LDH/NF, MoP@NiCo-LDH/NF-20, and Pt/C/NF towards HER are 495, 419, 326, 373, 255, and 170 mV. The Tafel slopes of NF, MoP/NF, NiCo-LDH/NF, MoP@NiCo-LDH/NF-20, and Pt/C/NF towards HER are 189, 171, 152, 165, 145, and 49 mV dec^{-1}. The driving voltages of MoP/NF||MoP/NF, NiCo-LDH/NF||NiCo-LDH/NF, MoP@NiCo-LDH/NF-20||MoP@NiCo-LDH/NF-20, and Pt/C/NF||IrO_2/NF are 1.494, 1.579, 1.405, and 1.708 V. The C_{dl} values of

MoP/NF||MoP/NF, NiCo-LDH/NF||NiCo-LDH/NF, and MoP@NiCo-LDH/NF-20||MoP@NiCo-LDH/NF-20 are 35.3, 10.1, and 70.1 $mF \cdot cm^{-2}$. The R_{ct} values of MoP/NF||MoP/NF, NiCo-LDH/NF||NiCo-LDH/NF, and MoP@NiCo-LDH/NF-20||MoP@NiCo-LDH/NF-20 are 5.1, 7.3, and 3.2 Ω. It is clear that only when MoP, NiCo-LDH, and NF are combined at the same time, will the material have the best catalytic performance and be superior to the noble metal catalyst (IrO_2/NF and Pt/C/NF). And the two-electrode electrolyser MoP@NiCo-LDH/NF-20||MoP@ NiCo-LDH/NF-20 has the best catalytic performance.

Ⅶ. Comparison of the catalytic performance for several recently reported catalysts at 100 mA cm^{-2}.

Table S2 shows the comparison of the catalytic performance for several recently reported catalysts at 100 mA cm^{-2} (potentials vs. RHE). The potentials of MoP@NiCo-LDH/NF-20 for UOR, HER, and cell in 1.0 M KOH with 0.5 M urea are 1.392 V, 255 mV, and 1.31 V. The potentials of HC-NiMoS/Ti for UOR, HER, and cell in 1.0 M KOH with 0.33 M urea are 1.40 V, 180 mV, and 1.80 V. The potentials of NiFeCo-LDH/NF for UOR, HER, and cell in 1.0 M KOH with 0.33 M urea are 1.438 V, 252 mV, and 1.64 V. The potentials of $Fe_xCo_{2-x}P$/NF for UOR, HER, and cell in 1.0 M KOH with 0.5 M urea are 1.40 V, 208 mV, and 1.62 V. The potentials of Ni-Co_9S_8/CC for UOR, HER, and cell in 1.0 M KOH with 0.33 M urea are 1.44 V, 300 mV, and 1.73 V. The potentials of Ni_2P/Fe_2P/NF for UOR, HER, and cell in 1.0 M KOH with 0.5 M urea are 1.46 V, 340 mV, and 1.68 V. The potentials of $Co_{0.26}$-$Ni(OH)_2$/CF for UOR, HER, and cell in 1.0 M KOH with 0.5 M urea are 1.38 V, 230 mV, and 1.64 V. The potentials of $Fe_{11.1\%}$-Ni_3S_2/NF for UOR, HER, and cell in 1.0 M KOH with 0.33 M urea are 1.439 V, 250 mV, and 1.80 V. The potentials of $NiCo_2S_4$/CC for UOR, HER, and cell in 1.0 M KOH with 0.33 M urea are 1.55 V, 310 mV, and 1.60 V. The potentials of Ni_3N/CC for UOR, HER, and cell in 1.0 M KOH with 0.33 M urea are 1.53 V, 350 mV, and 1.68 V. The potential of CoFeCr LDH/NF for UOR in 1.0 M KOH with 0.33 M urea is 1.41 V. The potentials of Ni_3N/N for UOR, HER, and cell in 1.0 M KOH with 0.5 M urea are 1.40 V, 250 mV, and 1.42 V. The potentials of N-NiS/NiS_2 for UOR, and cell in 1.0 M KOH with 0.33 M urea are 1.42 V, and 1.52 V. Obviously, the potential of MoP@NiCo-LDH/NF-20 is lower than that of the other catalysts, indicating its activity is the best.

Table S2 Comparison of the catalytic performance for several recently reported catalysts at 100 mA cm^{-2}.

Catalysts	Electrolyte	UOR	HER	Cell	Refs.
		Potential (V)	Potential (mV)	Voltage (V)	
MoP@NiCo-LDH/NF-20	1.0 M KOH with 0.5 M urea	1.392	255	1.31	This work
HC-NiMoS/Ti	1.0 M KOH with 0.33 M urea	1.40	180	1.80	1
NiFeCo-LDH/NF	1.0 M KOH with 0.33 M urea	1.438	252	1.64	2
$Fe_xCo_{2-x}P$/NF	1.0 M KOH with 0.5 M urea	1.40	208	1.62	3
Ni-Co_9S_8/CC	1.0 M KOH with 0.33 M urea	1.44	300	1.73	4
Ni_2P/Fe_2P/NF	1.0 M KOH with 0.5 M urea	1.46	340	1.68	5
$Co_{0.26}$-$Ni(OH)_2$/CF	1.0 M KOH with 0.5 M urea	1.38	230	1.64	6
$Fe_{11.1\%}$-Ni_3S_2/NF	1.0 M KOH with 0.33 M urea	1.439	250	1.8	7
$NiCo_2S_4$/CC	1.0 M KOH with 0.33 M urea	1.55	310	1.60	8
Ni_3N/CC	1.0 M KOH with 0.33 M urea	1.53	350	1.68	9
CoFeCr LDH/NF	1.0 M KOH with 0.33 M urea	1.41	-	-	10
Ni_3N/NF	1.0 M KOH with 0.5 M urea	1.40	250	1.42	11
N-NiS/NiS_2	1.0 M KOH with 0.33 M urea	1.42	-	1.62	12

Ⅷ CV curves and estimated C_{dl} values of MoP/NF, NiCo-LDH/NF, and MoP@NiCo-LDH/NF-x

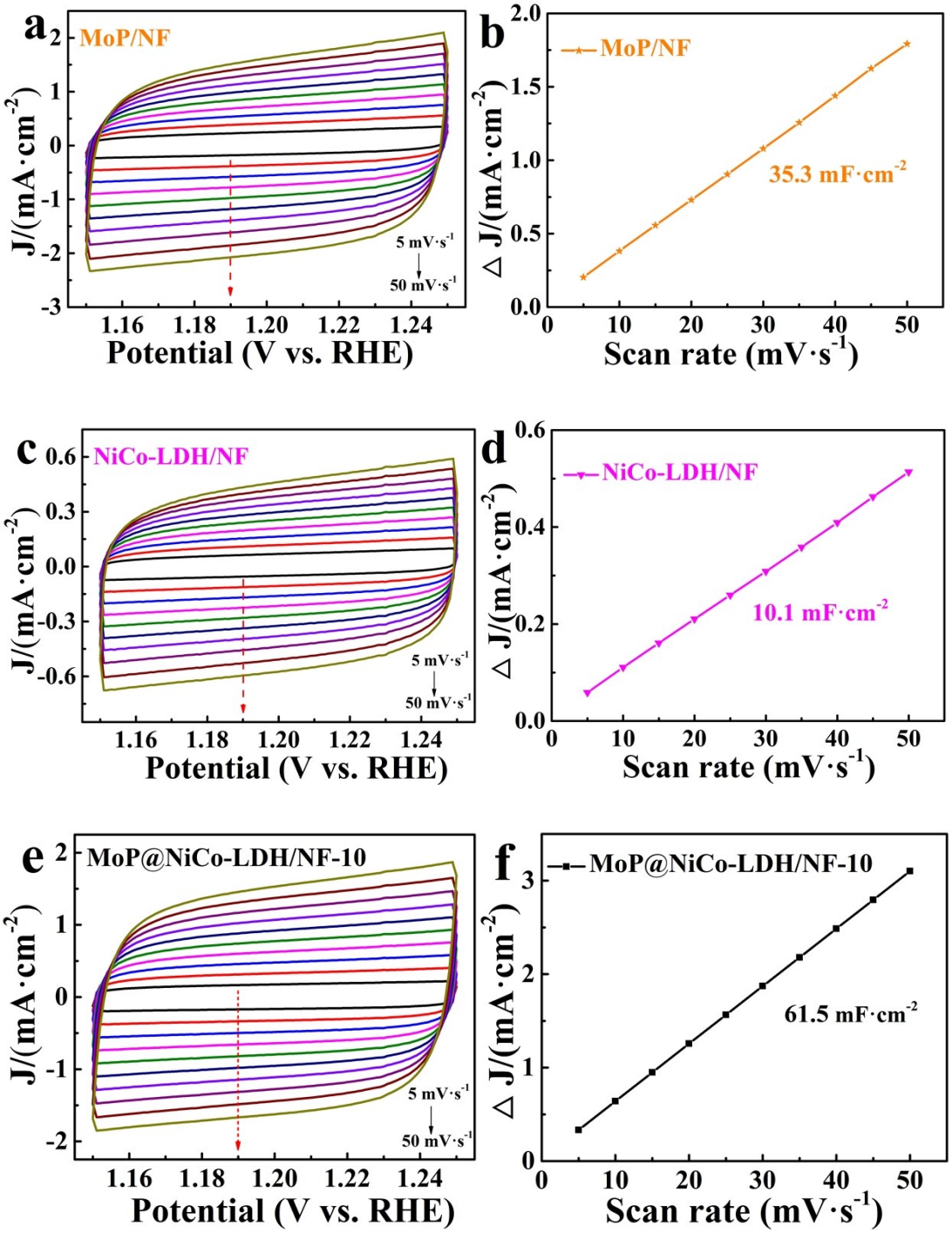

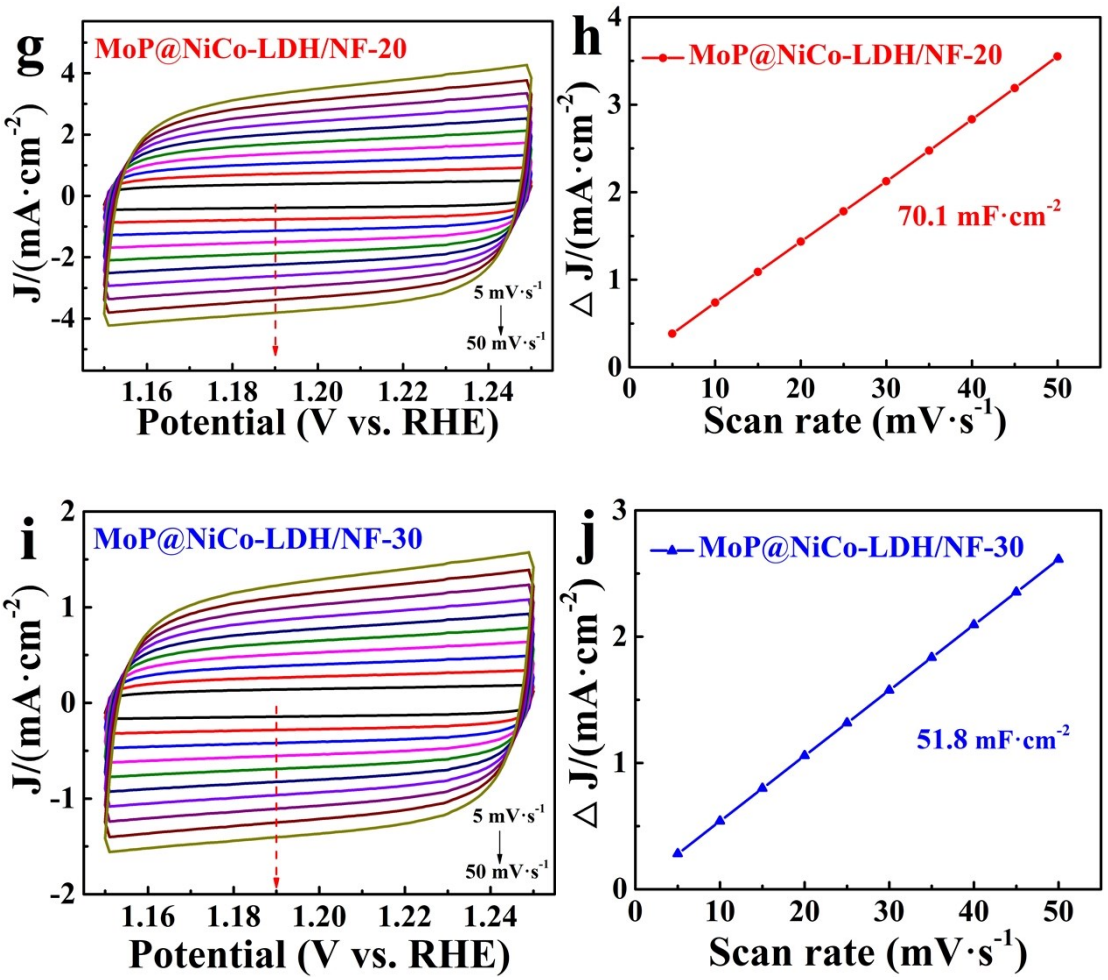

Figure S6. CV curves (a-c) and estimated C_{dl} values from the corresponding relationship between the current at 1.19 V and the scan rate (d-f) of MoP/NF, NiCo-LDH/NF, and MoP@NiCo-LDH/NF-x in 1.0 M KOH with 0.5 M urea, respectively.

Figure S6 (a, c e, g and i) shows CV curves of MoP/NF, NiCo-LDH/NF, and MoP@NiCo-LDH/NF-x from 5 to 50 mV s^{-1}. As the sweep speed increases, the current density increases. **Figure S6 (b, d, f, h, and j)** shows C_{dl} values of MoP/NF, NiCo-LDH/NF, and MoP@NiCo-LDH/NF-x from the corresponding relationship between the current density difference and the scan rates from 5 to 50 mV s^{-1} in 1.0 M KOH with 0.5 M urea (at 1.19 V). It can be measured by the cyclic voltammetry (CV). The figures presented different catalyst MoP/NF, NiCo-LDH/NF, and MoP@NiCo-LDH/NF-x (x=10, 20, and 30 minutes) corresponding C_{dl} values are

35.3, 10.1, 61.5, 70.1, and 51.8 mF cm^2. Obviously, the MoP@NiCo-LDH/NF-20 with maximum C_{dl}, showing that it has a larger specific surface area, this may be due to the special catalyst materials related to the morphology. Fold lamella tremella clusters with greater specific surface area, compared to NiCo-LDH/NF, have more active sites exposure due to the coordination of polymetallic compounds in the design and synthesis process.

Ⅸ SEM, TEM, and STEM-EDX mapping images of MoP@NiCo-LDH/NF-20 after electrolysis for 20 hours

Figure S7 shows SEM, TEM, and STEM-EDX mapping images of MoP@NiCo-LDH/NF-20 after electrolysis for 20 hours in 1 M KOH with 0.5 M urea. As shown in figure, the catalyst after electrolysis still presents a folded lamellar tremella, and all the elements are evenly distributed. By comparing SEM, TEM and scanning maps before electrolysis (**Figure 3**), it is found that after electrolysis, the physical morphology of the catalyst hardly changes, indicating the durability of the catalyst.

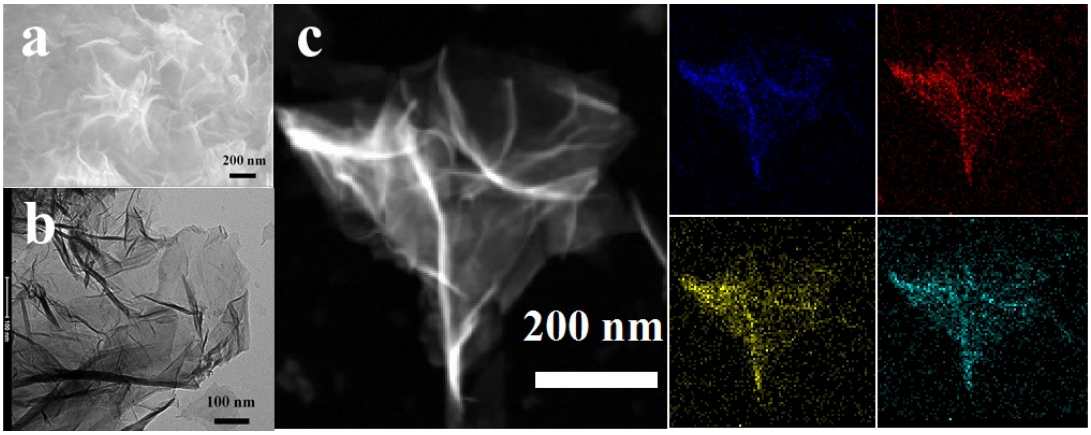

Figure S7. SEM, TEM, and STEM-EDX mapping images of MoP@NiCo-LDH/NF-20 after electrolysis for 20 hours in 1 M KOH with 0.5 M urea.

X XPS of Mo 3d, P 2p, Ni 2p, and Co 2p elements of MoP@NiCo-LDH/NF-20 after long-term urea-water electrolysis

Figure S8 shows XPS spectra of Mo 3d (a), P 2p (b), Ni 2p (c), and Co 2p (d) elements of MoP@NiCo-LDH/NF-20 after long-term urea-water electrolysis in 1 M KOH with 0.5 M urea. Even though the diffraction peaks are slightly offset, they still correspond to their respective substances. As can be seen from the figure, the peak before and after electrolysis is not significantly offset.

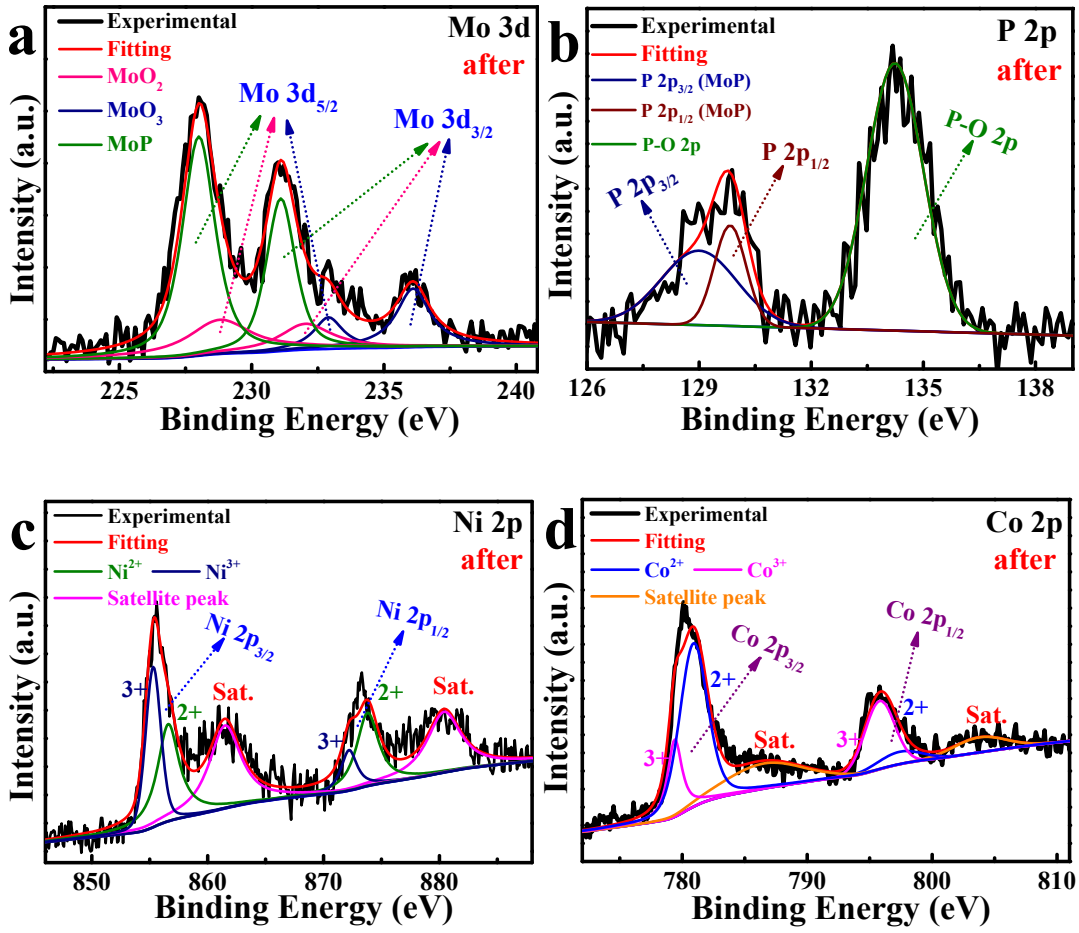

Figure S8. XPS spectra of Mo 3d (a), P 2p (b), Ni 2p (c), and Co 2p (d) elements of MoP@NiCo-LDH/NF-20 after long-term urea-water electrolysis in 1 M KOH with 0.5 M urea.

Reference

1 X. X. Wang, J. M. Wang, X. P. Sun, S. Wei, L. Cui, W. R. Yang and J. Q. Liu, *Nano Research*, 2018, **11**, 988-996.

2 P. Babar, A. Lokhande, V. Karade and B. Pawar, *ACS Sustainable Chemistry & Engineering*, 2019, **7**, 10035-10043.

3 T. I. Singh, G. Rajeshkhanna, S. B. Singh, T. Kshetri, N. H. Ki and J. H. Lee, *ChemSusChem*, 2019, **12**, 4810-4823.

4 P. Hao, W. Q. Zhu, L. Y. Li and J. Tian, *Electrochimica Acta*, 2020, 338, 135883.

5 L. Yan, Y. L. Sun, E. L. Hu and J. Q. Ning, *Journal of colloid and interface science*, 2019, **541**, 279-286.

6 C. B. Sun, M. W. Guo, S. S. Siwal and Q. B. Zhang, *Journal of Catalysis*, 2020, **381**, 454-461.

7 W. X. Zhu, Z. H. Yue, W. T. Zhang and N. Hu, *Journal of Materials Chemistry A*, 2018, **6**, 4346-4353.

8 W. X. Zhu, M. R. Ren, N. Hu and W. T. Zhang, *ACS Sustainable Chemistry & Engineering*, 2018, **6**, 5011-5020.

9 Q. Liu, L. S. Xie, F. L. Qu, Z. A. Liu, G. Du, A. M. Asiri and X. P. Sun, *Inorganic Chemistry Frontiers*, 2017, **4**, 1120-1124.

10 Z. L. Wang, W. J. Liu, Y. M. Hu, M. L. Guan, L. Xu, H. P. Li, J. Bao and H. M. Li, *Applied Catalysis B: Environmental*, 2020, **272**, 118959.

11 S. N. Hu, C. Q. Feng, S. Q. Wang, J. W. Liu, H. M. Wu, L. Zhang and J. J. Zhang, *ACS Appl. Mater. Interfaces*, 2019, **11**, 13168−13175.

12 H. Liu, Z. Liu, F. L. Wang and L. G. Feng, *Chemical Engineering Journal*, 2020, **397**, 125507.